A communication-free reactive-power control strategy in VSC-HVDC multi-terminal systems to improve transient stability

Javier Renedo, Luis Rouco, Aurelio García-Cerrada, and Lukas Sigrist
Instituto de Investigación Tecnológica (IIT), ETSI ICAI, Universidad Pontificia Comillas, Madrid, Spain
(e-mail: javier.renedo@iit.comillas.edu; luis.rouco@iit.comillas.edu; aurelio@iit.comillas.edu; lukas.sigrist@iit.comillas.edu)

Abstract

This paper proposes a new reactive-power control strategy for High Voltage Direct Current multi-terminal systems with Voltage Source Converter stations (VSC-HVDC) to improve transient stability in electric power transmission systems. The proposed algorithm uses local measurements to estimate, in each converter station, a weighted average of the frequencies seen by the VSC stations of the HVDC multi-terminal system. This estimation is carried out making use of a (small) auxiliary local active-power modulation along with the DC-side voltage droop control in the VSC stations, where the latter also uses local measurements only. The estimated frequency is used as the set point for supplementary reactive-power control at each converter station. The proposed control law has been simulated in a test system using PSS/E and the results show that it improves transient stability, significantly, producing similar results to those obtained controlling reactive power using global measurements.

Index Terms

VSC HVDC, multi-terminal, transient stability, reactive power control, power systems, local measurements.

This is an unabridged draft of the following paper:

- J. Renedo, L. Rouco, A. García-Cerrada, L. Sigrist, *"A communication-free reactive-power control strategy in VSC-HVDC multi-terminal systems to improve transient stability,"* Electric Power Systems Research, vol. 174, 105854, pp. 1-13, 2019.

Internal reference of this paper:

- IIT-17-005A (www.iit.comillas.edu)

I. Introduction

Electrical grids in Europe are expected (a) to ease the integration of local distributed generation, (b) to integrate remote renewable generation such as a large amount of offshore wind power from the North Sea and (c) to connect to neighbouring electrical systems such as the Baltic Energy Market or those in African Countries [1]. To make this possible, it is necessary to increase the transmission capability of the system, interconnect power systems of different countries (even asynchronous) and be able to transmit, efficiently, distant offshore energy to the onshore grid through submarine cables. Meanwhile, the reinforcement of the existing infrastructure with new overhead AC lines raises important environmental concern and public opposition and Transmission System Operators (TSOs) are often driven to plan for underground connections. High Voltage Direct Current (HVDC) technology has a great potential to tackle these challenges, above all if submarine or underground cables are required. HVDC based on Line Commutated Converters (LCC-HVDC) is already a mature technology while multi-terminal HVDC systems based on Voltage Source Converters (VSC-HVDC) have many advantages as pointed out in [2], for example. Unfortunately, the latter is less mature and more expensive than the former and it is necessary to investigate further whether its potential advantages can overweight its investment costs.

When planing to stretch power systems to their transmission limits, transient stability (i.e, the ability of the generators to remain in synchronism after large disturbances [3]) is one of the most important limiting factors. Although bulk power transmission should remain the main purpose of any multi-terminal VSC-HVDC system (VSC-MTDC, for short) to be built, they are also a very attractive alternative to improve transient stability, due to the fast control of active- and reactive-power injections of the VSC stations at different (often distant) points [4], [5]. In fact, previous publications have shown that transient stability could be greatly improved using VSC-HVDC point-to-point links [6]–[9] and VSC-HVDC multi-terminal systems [10]–[14]. A complete review of previous work on control strategies in VSC-MTDC systems with a detailed description of each strategy is presented in Subsection I-A.

A. Previous work

The work reported in [11] proposed a control strategy for active-power (P) injections of VSC stations in VSC-MTDC systems to improve transient stability. Supplementary P set points were calculated using the deviation of the speed of each generator of the system with respect to the speed of the centre of inertia (COI) and a similar approach is reported in [13]. More recently, [12] showed that transient stability could be improved if supplementary P set points at each VSC was made proportional to the deviation of the frequency measured at the AC side of the VSC with respect to a weighted average of the frequencies (WAF, for short) measured at all the stations of the VSC-MTDC system. The calculation of the WAF requires communications among the converters, but the procedure is easier than the one proposed in [11] because VSC frequencies are already available for synchronisation of the stations with the grid. The results of the proposal in [12] were there compared with those in [11] showing similar improvements. A different control strategy for P injections of the VSC stations in a MTDC system based on operating point adjustment was proposed to improve transient stability in [15], based on a wide-area measurement system (WAMS). While the strategies in [11]–[13] only modulate P injections during the transients, in [15], the VSC stations reach a new operating point.

The work in [10] addressed P and reactive-power (Q) modulation to improve transient stability. Two areas connected by a VSC-MTDC system were considered and the additional power set points for each converter station were calculated using the deviation of the speeds of all generators of each area. The individual contribution of the P and Q modulation is not explained clearly in [10]. ENTSO-E requires Fault Ride Through (FRT) capability for generators and converters connected to the grid, according to corresponding TSO requirements [16], [17]. Often TSOs require to maintain the converter connected during voltage sags and to provide voltage support during the fault (using local measurements) [18]. Along this line, the work in [19] investigated local fast voltage support controllers at the VSC stations of an MTDC, to improve transient stability. However, further improvements in multi-machine systems may be expected using global measurements [7], [9]. More recently, a control strategy for Q injections of the VSC stations in an MTDC system was proposed in [14], where results show that transient stability can be greatly improved if if supplementary Q set points for VSC stations are calculated as in [12]: using the deviation of the frequency measured at each converter station with respect to the weighted-average frequency of the VSC-MTDC system. The strategy proposed in [14] is a generalisation of the idea presented in [8] where

the frequency difference between the two stations of a VSC-HVDC link was used to control Q injections of the converter stations to improve the transient stability. When comparing [10] with [14], results showed that the improvement in the former was probably due to P modulation rather than to Q modulation. Again, the use of the WAF required communication among the stations of the MTDC system and, this time, the control using Q proved to be less robust than using P when the effects of communication delays were investigated. The work in [20] proposed a control strategy for P and Q injections in VSC-MTDC systems connecting offshore wind farms for transient stability improvement. P and Q injections of the onshore converters and P injections of the wind farms (offshore converters) where calculated as a function of the speed deviations of the generators with respect to the COI. This strategy produces significant improvements. However, again, a disadvantage is the need of a WAMS to be able to obtain the speeds of all generators of the system in real time.

Summarising, effective control strategies in VSC-MTDC systems to improve transient stability have three important aspects in common:

1) Converters determine their control actions by using global measurements and centralised control schemes.
2) The system's global behaviour is analysed through frequency-related measurements such as the speed of several/all generators or the frequency measurements at the AC side of the converter stations.
3) The control actions take the form of active- and/or reactive-power modulation around the power set points established by the TSOs to shape the power flows in the system.

B. Contributions of this paper

Results show that using global measurements is a richer and more efficient approach than looking at local information only. This is due to the fact that transient stability is a global problem which involves synchronism between synchronous machines located at different points of the system. Control strategies using global measurements are much more effective to prevent loss of synchronism, since they depend on the global behaviour of the system, aiming to pull together rotor-angle difference between synchronous machines of the system. Nevertheless, the use of global information requires a communication system that could be subject to delays and even failures. This paper deals with obtaining global information of a VSC-MTDC system by using local information at each converter station, only, and using this information for transient-stability-tailored control strategies.

A well-known technique to obtain global information by using local information in DC microgrids is the concept of *DC-bus signaling* [21], [22]. The idea of DC-bus signaling is to change the voltage of the DC grid, so that other converters can perform control actions depending on global information, but avoiding a communication system among the converters. Although this concept has not been used for HVDC applications so far, some examples in VSC-MTDC systems implicitly use voltage through the DC grid as an information carrier. The most common example is the so called DC-voltage droop [23]–[26]: under a power imbalance, converters distribute power contribution according to their DC-voltage droop constants. Furthermore, previous control strategies for frequency support among different asynchronous AC areas through VSC-MTDC systems also prove (implicitly) that global information can be obtained using local measurements [27]–[30]. In those strategies, a local frequency droop and a DC-voltage droop were implemented together at each VSC station. As a result of the interaction of the AC- and DC-side strategies, the healthy areas can support the faulted ones through the VSC-MTDC system, using local measurements, only. Finally, the work in [31] proposed a local control strategy for VSC-MTDC systems to damp power oscillations and its effectiveness is due to the fact that information is propagated through the voltages of the DC grid.

Inspired by this behaviour, this paper proposes a new reactive-power control strategy at the VSC stations of an MTDC system to improve transient stability in HVAC/HVDC hybrid systems, using local measurements. Specifically, the contributions of this paper as follows:

- A new communication-free control strategy for reactive-power injections in VSC-MTDC systems to improve transient stability.
- A new method by means of which a VSC station can estimate the weighted-average frequency at the AC terminals of a VSC-MTDC system, using local measurements. This estimation can then be used by the proposed local control strategy. Nevertheless, it may be of interest for other applications.
- Results will show that the proposed strategy performs reasonable well when compared to reactive-power modulation based on the use of global information.

- The proposed control strategy is based on the reactive-power control strategy previously proposed in [14], which uses the weighted average of the frequencies measured at the AC side of the VSC stations as set point value for supplementary reactive-power control. Instead, in the proposed local control strategy each converter estimates the weighted-average frequency by using local measurements and this estimation is used as set-point value for reactive-power control. Therefore, a communication system can be avoided. Furthermore, if a communication system is already available, the proposed control strategy could also be of interest if communication latencies are too high or as a back-up control strategy when communication fails.

C. Organisation of the paper

This paper is organised as follows. Section I reviews the literature of active- (P) and reactive-power (Q) control strategies for VSC-MTDC systems, specially those tailored to improve transient stability, and identifies the contributions of this paper. Section II describes VSC-MTDC systems, their models and the implementation of supplementary control strategies. Section III presents the proposed local Q-control strategy. Section III-A describes the proposed Q-control strategy based only on local measurements. How those local measurements can be used to obtained system-wide information is described in Sections III-B and guidelines for the design are provided in III-C. Section IV presents an illustrative example, which consists of Kundur's two-area test system with an embedded VSC-MTDC, in order to described, in detail, the performance of the proposed local control strategy. Results in a larger case study (Nordic32A test system + a VSC-MTDC) are shown and discussed in Section V. Finally, the conclusions of the study are summarised in Section VI. Data of the test systems used and a description of additional control strategies used for further comparison are presented in the Appendix.

II. VSC-HVDC MULTI-TERMINAL SYSTEMS

A VSC-MTDC system consists of more than two VSC stations connected to the same DC grid. The dynamic model of a VSC station, including its connection to the AC side and the DC grid, is depicted in Fig. 1 [32]–[34], where:

1) Each VSC is connected to the AC grid through a low-pass filter ($r_{c,i}$, $L_{c,i}$ and $C_{f,i}$) and a transformer ($r_{tf,i}$ and $L_{tf,i}$). It is, usually, current controlled using a vector-control strategy on a synchronously-rotating frame dq with the d axis aligned with the AC voltage space vector at the connection point ($\bar{u}_{s,i}$). The d-axis current can be used to control the active power or the DC voltage, whilst the q-axis current can be used to control the reactive power or the modulus of the AC voltage. Current limiter of VSC stations is set to P-control priority in this work.
2) DC grid: It contains the DC cables, the DC side of each converter and the equivalent DC capacitor of each converter ($C_{VSC,i}$). The DC lines are represented by a series resistance ($R_{dc,ij}$), a series inductance ($L_{dc,ij}$) and a shunt capacitance at each end ($C_{cc,ij}/2$). The DC side of a converter is modelled as a current injection ($i_{dc,i}$). The total capacitance of each DC bus, $C_{dc,i}$, is the sum of the equivalent capacitor of the VSC plus the contribution of the capacitance of the DC lines connected to that bus.
3) AC/DC coupling: The AC and DC sides of a VSC-i are coupled by the energy conservation principle: $p_{c,i} + p_{loss,i} + p_{dc,i} = 0$, where the losses of the converters are approximated by a quadratic function of the converter current $i_{c,i}$ (rms), as proposed in [35], $p_{loss} = a + b \cdot i_c + c \cdot i_c^2$ and $p_{c,i}$ and $p_{dc,i}$ are the active power injections in the AC and in the DC systems, respectively.

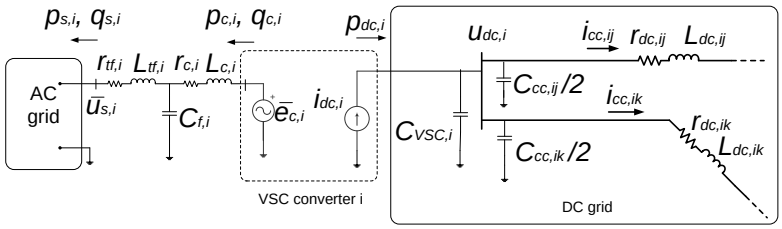

Fig. 1: Model of a VSC and the DC grid [32].

The control of active- (P) and reactive-power (Q) injections in each VSC station of an MTDC system is summarised in Fig. 2 where the power set points established by the TSOs are p_s^0 for the active power and q_s^0 for reactive power while the supplementary P and Q set points, related to transient stability improvement, are Δp_s^{ref} and Δq_s^{ref}, respectively. The P set point eventually used in the VSC stations (p_s^{ref}) is further modified to help maintaining a constant DC voltage (u_{dc}) close to its set-point value (u_{dc}^0) using a proportional control strategy known as DC-voltage droop ($1/k_{dc}$). The actual P error ($p_s^{ref} - p_s$) and Q error ($q_s^{ref} - q_s$) are used by two independent controllers to generate the references for the converter d-axis and q-axis currents ($i_{s,d}^{ref}$ and $i_{s,q}^{ref}$, respectively) which will be tackled by an inner control layer at the AC side of each VSC.

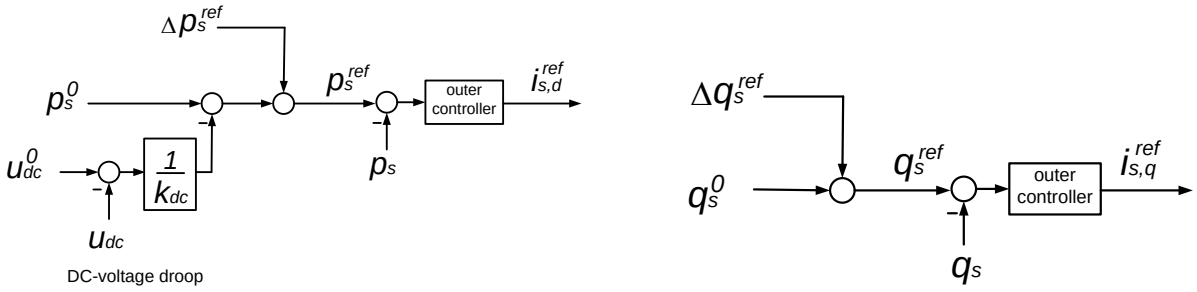

(a) (b)

Fig. 2: (a) P control and (b) Q control.

III. Q CONTROL FOR TRANSIENT STABILITY IMPROVEMENT USING LOCAL MEASUREMENTS

A. Reactive-power control

A Q controller for a converter station as proposed in [14] is depicted in Fig. 3. The supplementary Q injection, tailored to improve transient stability (Δq_s^{ref}), is derived, with a proportional action, (k_Q) from the error between the frequency set point (ω^*) and the actual frequency measured at the station AC terminals (ω). The error is filtered by a low-pass filter (with a time constant T_f) and passes through a wash-out block with unity high-frequency gain and a time constant T_W. The wash-out filter prevents the use of the supplementary injection in steady state. A binary variable, γ, is used to activate the controller depending on the conditions, if desired. Notice that Δq_s^{ref} is positive (negative) when the measured frequency is above (below) its set point. The transfer function of the supplementary Q set point reads:

$$\Delta q_s^{ref}(s) = (-1) \cdot \left(\frac{k_Q}{1+sT_f}\right)\left(\frac{sT_W}{1+sT_W}\right) \tag{1}$$

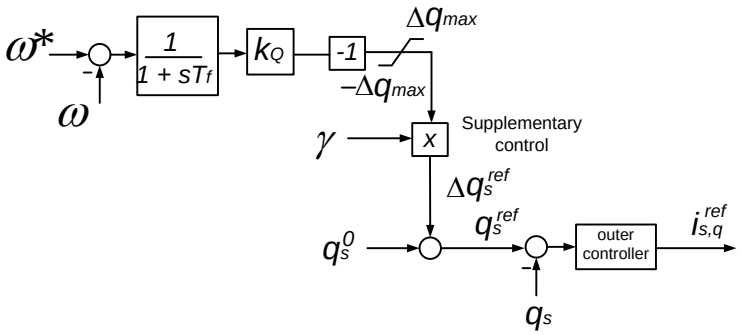

Fig. 3: Control for the reactive-power injection of a VSC.

In the communication-based strategy proposed in [14],which was called Q-WAF (Q Weighted Average Frequency), ω^* in Fig. 3 was calculated as:

$$\bar{\omega} = \sum_{k=1}^{n} \alpha_k \omega_k, \quad \begin{cases} \alpha_k \in [0,1] \\ \sum_{k=1}^{n} \alpha_k = 1 \end{cases} \tag{2}$$

Unlike with active-power injections of the converters, it is not mandatory to guarantee a net reactive-power injection equal zero in a VSC-MTDC system. Nevertheless, good results have been obtained choosing the frequency-averaging weights as follows:

$$\alpha_k = \frac{k_{Q,k}}{k_{Q,T}}, \;\; k_{Q,T} = \sum_{j=1}^{n} k_{Q,j}, \quad \left(\rightarrow \text{ensuring that } \sum_{j=1}^{n} \Delta q_j^{ref} = 0\right) \tag{3}$$

The idea behind the use of the WAF ($\bar{\omega}$ in (2)) in Q control in a VSC-MTDC system is to pull generator speeds together by accelerating those which are running slower and decelerating those which are running faster, which has proved to be a key aspect in control strategies for transient stability improvement [36]–[38]. Increasing (reducing) Q injections will increase (reduce) the electromagnetic torque seen by nearby generators causing the deceleration (acceleration) of those generators. Physically, Q injections of the VSCs are directly related to the electromagnetic torque seen by synchronous machines because they modify the voltages of the system and, therefore, they modify the electrical power of generators.

In order to avoid having to use communications to calculate (2), this paper proposes to estimate $\bar{\omega}$ using local measurements only, based on the experience of modulating P to improve transient stability. The estimation will be used by each converter as its frequency set point. This Q-control strategy will be called Q-LWAF (Q Locally estimated Weighted Average Frequency), for short, in the rest of the paper.

B. Estimation of the weighted-average frequency (WAF) using local measurements

Each VSC station will estimate the weighted-average frequency (WAF) of the MTDC system (2) using local measurements, by means of an auxiliary local active-power control strategy. In this method, voltages through the DC grid are used as a communication carriers instead of using a communication system. This novel idea was inspired in results obtained in previous work [12], [27]–[30].

Active-power (P) set point Δp_s^{ref} in Fig. 2 was used in [12] to improve transient stability in an AC power system with an embedded VSC-MTDC system. This set point was calculated as in Fig. 4 where a low-pass filter and a wash-out block were included resembling Fig. 3 and ω^* was calculated as $\bar{\omega}$ in (2) (strategy P-WAF, for short) or was made equal to 1 p.u (strategy P-LF, for short).

As shown in [12], theoretically, both strategies (P-WAF and P-LF) should produce similar results if k_P and k_{dc} of each converter and α_k in (2) are chosen appropriately. However, simulation results in [12] showed that:

- For severe faults, global strategy P-WAF and local strategy P-LF behave differently and the former was much more effective to improve transient stability. Local strategy P-LF presented poor results against severe faults due to DC-voltage fluctuations, which drove some converters to reach their DC-voltage limits.
- For less-severe faults, global strategy P-WAF and local strategy P-LF produce similar results. This is because DC-voltage limits of the converters are not reached.

Since using $\omega^* = 1$ p.u. only involves local measurements, a (small) active-power (P) modulation (strategy P-LF) can be included in each converter station to be able to estimate the weighted-average frequency (WAF) of the VSC-MTDC system to be used as frequency set point of strategy Q-LWAF (Fig. 3). This is possible because of the interaction of the AC-side control strategy and the DC-voltage droop (Fig. 4), which allows local strategy P-LF to behave similar to global strategy P-WAF. This is only true if DC-voltage limits are not reached. Since local strategy P-LF will be used for estimation purposes only (and not for transient stability improvement), small gains $k_{P,i}$ can be used and DC-voltage deviations produced by local strategy P-LF would not be very severe. The estimation process can be described as follows.

From Fig. 4:

$$p_{s,i}^{ref}(t) \;=\; p_{s,i}^0 - \frac{1}{k_{dc,i}}(u_{dc,i}^0 - u_{dc,i}(t)) + \Delta p_{s,i}^{ref}(t) = p_{s,i}^0 + \underbrace{\Delta p_{s,i}^{ref,DC}(t) + \Delta p_{s,i}^{ref}(t)}_{\Delta p_{s,i}^*(t)} \tag{4}$$

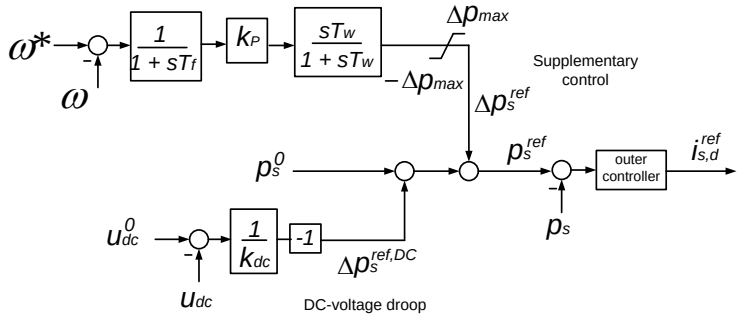

Fig. 4: Control for the active-power injection of a VSC.

Let's assume that strategy P-LF (Fig. 4 with $\omega_i^* = \omega_0 = 1$ p.u.) is implemented in each converter of a VSC-MTDC system using small gains ($k_{P,i}$) in order to produce a small P modulation. Let's also assume that,

$$\alpha_k = \frac{k_{P,k}}{k_{P,T}} = \frac{1/k_{dc,k}}{1/k_{dc,T}}, \quad \text{with} \quad k_{P,T} = \sum_{j=1}^{n} k_{P,j} \quad \text{and} \quad \frac{1}{k_{dc,T}} = \sum_{j=1}^{n} \frac{1}{k_{dc,j}}. \tag{5}$$

With a DC-voltage droop scheme in place, converters will react against a steady-state active-power imbalance in the VSC-MTDC system [30], [39]. This mechanism will be activated, for example, when the converters slowly change their P injections due to variations in the system frequency. Hence, the active-power supplementary reference

associated to the DC-voltage droop of (4) can be written as a function of the AC active-power supplementary set point as:

$$\Delta p_{s,i}^{ref,DC} \simeq -g_i \underbrace{\Big(\sum_{k=1}^{n} \Delta p_{s,k}^{ref}\Big)}_{\Delta p_{total}^{ref}}, \quad g_i = \frac{1/k_{dc,i}}{\sum_{k=1}^{n} 1/k_{dc,k}}. \tag{6}$$

Notice that the design in (5) implies $g_i = \alpha_i$.

Within the bandwidth of the controller and if no limits are reached, the supplementary set point using strategy P-LF is $\Delta p_{s,i}^{ref} \simeq k_{P,i}(\omega_0 - \omega_i)$. Hence, the total active-power supplementary set point can be manipulated as:

$$\begin{aligned} \Delta p_{s,i}^{*} &= \Delta p_{s,i}^{ref} + \Delta p_{s,i}^{ref,DC} \simeq \Delta p_{s,i}^{ref} - g_i\Big(\sum_{k=1}^{n} \Delta p_{s,k}^{ref}\Big) \\ &= k_{P,i}(\omega_0 - \omega_i) - g_i\Big[\sum_{k=1}^{n} k_{P,k}(\omega_0 - \omega_k)\Big] = g_i k_{P,T} \sum_{k=1}^{n} \frac{k_{P,k}}{k_{P,T}}\omega_k - k_{P,i}\omega_i + k_{P,i}\omega_0 - g_i k_{P,T}\omega_0 \end{aligned} \tag{7}$$

and using the conditions in (5),

$$\Delta p_{s,i}^{*} \simeq k_{P,i}(\bar{\omega} - \omega_i) \tag{8}$$

where $\bar{\omega}$ is given by (2) and the weights verify (5). Hence, each converter can estimate the weighted-average frequency (using local measurements) as:

$$\bar{\omega}_{e,i} = \omega_i + \frac{\Delta p_{s,i}^{*}}{k_{P,i}} \simeq \bar{\omega} \tag{9}$$

where, for each converter i, ω_i is the frequency measured at the AC side, $\Delta p_{s,i}^{*}$ is the total active-power supplementary set point and $k_{P,i}$ is the gain used in strategy P-LF.

The estimated value of $\bar{\omega}_{e,i}$ can now be used by each VSC as its frequency set point for reactive-power modulation Q-LWAF. For estimation purposes $k_{P,i} = \alpha_i k_{P,T}$ need not be a big value. Control scheme Q-LWAF is like in Fig. 3 with $\omega_i^{*} = \bar{\omega}_{e,i}$ but, since the frequency set point is computed using internal signals already available from strategy P-LF (9), no additional field measurements are required to calculate the supplementary reactive-power command. Therefore, the low-pass filter T_f used for the reactive-power control scheme (Fig.3) could have a high cut-off frequency (~ 10ms) or could be eliminated.

However, if converters reach their current limit, the WAF could not be estimated properly during that instants of the transient. This is due to the fact that if a converter is blocking its current, it is not modulating P injections according to P-LF (auxiliary P control strategy), obviously. This can occur during faults close to VSC stations. In this cases, it is better to modulate Q once the fault is cleared. In order to achieve this, the proposed Q controller is only activated if the AC voltage at the connection point of the VSC is above a certain threshold ($\gamma = 1$ in Fig. 3 if $u_s \geq V_{TH}$ and $\gamma = 0$ otherwise).

C. Guidelines for the design of the controller

This section provides some practical guidelines for the design of the proposed control strategy Q-LWAF:

1) Q modulation (Fig. 3):
   - Gain values, $k_{Q,i}$, should be high enough to produce significant improvements on transient stability. Nevertheless, excessively high gain values can spoil results, since some converters might reach operation limits very often (during the fault and after the fault clearing). Good results were obtained with gain values within the range: $k_{Q,i} = [200, 300]$ p.u. (p.u referred to the converters' ratings) [14].
   - In this work, gain values of the converters, $k_{Q,i}$, verify (3), which produced good results. However, this condition is not mandatory.
   - A low-pass filter (with time constant $T_{f,i}$) is used to eliminate noise from frequency measurement and it should be in the range $T_{f,i} = [0.02, 0.1]$ s [14].

- A wash-out filter is used to avoid actuation of supplementary control under steady-state deviations and it is not critical from a dynamic point of view. Values for wash-out filter time constant are typically within the range $T_{W,i} = [1, 20]$ s [40].
- Saturation parameter, $\Delta q_{max,i}$, can take a large value (e.g. $\Delta q_{max,i} = 1$ p.u.), since converters will always have their own operation limits. However, smaller values of $\Delta q_{max,i}$ could be used to bound supplementary reactive-power injection of the VSCs, according to TSO's preferences.
- Voltage threshold to activate the supplementary Q controller. Reasonable values are within the range $V_{TH,i} = [0.50 - 0.85]$ p.u. ($\delta_i = 1$ if $u_{s,i} \geq V_{TH,i}$).

2) P modulation, for estimation purposes (Fig. 4 with $\omega^* = 1$ p.u.):

- Gain values, $k_{P,i}$, must be small, since auxiliary P control strategy is used to estimate the WAF. High values of $k_{P,i}$ would produce DC-voltage fluctuations. In practice, excessively low gain values might not be useful neither, due to dead band of the controllers. As a rule of thumb, gain values, $k_{P,i}$, should be small enough to avoid overvoltages in the DC grid, but high enough to be able to estimate the WAF successfully. Reasonable values of $k_{P,i}$ are within the range $k_{P,i} = [2 - 10]$ p.u.
- Weight values for the estimated WAF α_i, gain values $k_{P,i}$ and DC-voltage droop constants $k_{dc,i}$ must verify (5).
- Time constant $T_{f,i}$ can be small, since the input signal of this filter is an internal signal of the controller (and it is not a field measurement). Reasonable values for $T_{f,i}$ are within the range $T_{f,i} = [0, 0.05]$ s.
- Wash-out filter time constant are typically in the range $T_{W,i} = [1, 20]$ s [40].
- Saturation parameter, $\Delta p_{max,i}$, can take a large value (e.g. $\Delta p_{max,i} = 1$ p.u.).

Finally, it should be noted that, although other control strategies can be implemented using either centralised control of the voltage of the HVDC grid (with one DC-slack converter) or distributed control of the DC voltage (with DC-voltage droop control), in the proposed local control strategy, Q-LWAF, the use of -DC-voltage droop is mandatory, because the estimation of the WAF is possible due to the interaction of the AC-side auxiliary P-control strategy (P-LF, which is proportional to the frequency deviation) and the DC-voltage droop.

IV. Illustrative Example

The performance of the proposed control strategy (Q-LWAF) is illustrated in Kundur's two-area test system with an embedded VSC-MTDC system, as shown in Fig. 5. The power-flow algorithm and the dynamic model of the VSC-HVDC multi-terminal system have been implemented in PSS/E based on the guidelines in [32]–[34] (described in Section II). Data can be found in Section A-1 of the Appendix. Parameters of VSC stations and DC grid are provide in Table VI. The PSS/E model for VSC-HVDC multi-terminal system was validated in [41].

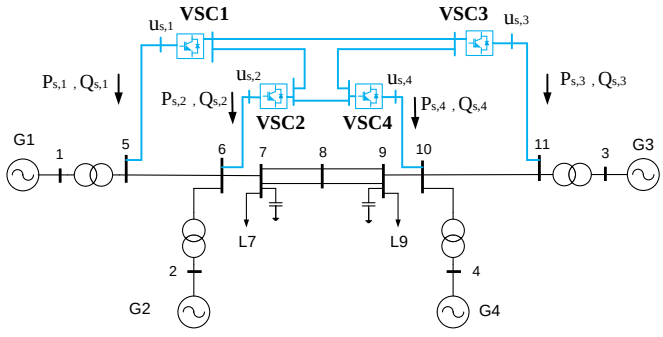

Fig. 5: Kundur's 2-area system with a VSC-MTDC.

The initial operating point of the MTDC system was set as:

- VSC1: $P^0_{s,1} = -200$ MW and $Q^0_{s,1} = 0$ MVAr.
- VSC2: $P^0_{s,2} = -200$ MW and $Q^0_{s,2} = 0$ MVAr.
- VSC3: $P^0_{s,3} = 200$ MW and $Q^0_{s,3} = 0$ MVAr.
- VSC4: $u^0_{dc,4} = 1$ p.u and $Q^0_{s,4} = 0$ MVAr (VSC4 is used as the DC-slack converter for power-flow calculation of the initial operating point).

The following control strategies will be compared:

- Q0: Constant reactive-power injections.
- Q-WAF: Reactive-power injection based on the weighted-average frequency of the converter stations (global measurement) (Fig. 3), with parameters: $k_{Q,i} = 200$ p.u, $T_{f,i} = 0.1$ s, $T_{W,i} = 15$ s, $\Delta q_{max,i} = 1$ p.u and $\alpha_k = 1/4$. The gains are in nominal p.u. The frequency set point is computed as (2).
- Q-LWAF: Reactive-power injection based on the estimated weighted-average frequency of the converter stations using local measurements, with parameters:
  - Q modulation (Fig. 3): $k_{Q,i} = 200$ p.u, $T_{f,i} = 0.01$ s, $T_{W,i} = 15$ s, $\Delta q_{max,i} = 1$ p.u, $V_{TH,i} = 0.80$ p.u and $\alpha_k = 1/4$. The frequency set point is computed as in (9).
  - P modulation, for estimation purposes (Fig. 4 with $\omega^* = 1$ p.u.): $k_{P,i} = 10$ p.u, $T_{f,i} = 0.1$ s, $T_{W,i} = 15$ s, $\Delta p_{max,i} = 1$ p.u and $k_{dc,i} = 0.1$ p.u. The frequency set point is $\omega_i^* = 1$ p.u (P-LF).

A. *Fault simulation*

A three-phase-to-ground fault at circuit a of line 7-8 has been simulated. The fault is cleared after 200 ms by disconnecting the faulted circuit. Figure 6 shows the angle difference between generators 1 and 3 (Fig. 5). Synchronism is lost with constant Q injections (Q0), while synchronism is maintained with global strategy Q-WAF and with the proposed local strategy Q-LWAF. Fig. 7 shows Q injections of the VSC stations, which follow a very similar pattern when using either Q-WAF or Q-LWAF. In these strategies, Q injections increase (decrease), during the transient, in those VSC stations with the frequency above (below) the weighted-average frequency (WAF), stabilising the system. Notice that maximum reactive power ($\pm$ 200 MVAr, Table VI) is reached the first milliseconds after the fault clearing.

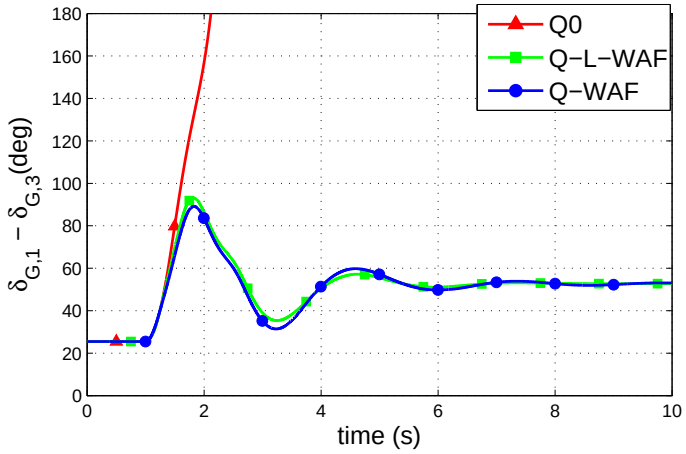

Fig. 6: Fault simulation. Generator angles.

Fig. 8 compares the WAF estimated by VSC1 ($\bar{\omega}_{e,1}$), using (9), with the true value ($\bar{\omega}$), and Fig. 9 compares the frequency deviation in VSC1, with respect to the true WAF ($\omega_1 - \bar{\omega}$) and with respect to the estimated WAF ($\omega_1 - \bar{\omega}_{e,1}$), showing good agreement (in Q-LWAF). Some high-frequency oscillations appear in the estimated signal $\bar{\omega}_{e,1}$ due to the DC-grid dynamics (see the inset of Fig. 8). The WAF cannot be estimated successfully during the fault, since converters reach their current limit and, therefore, the auxiliary P strategy cannot be implemented successfully. This is the reason for using a voltage threshold to activate Q-LWAF. Finally, Fig. 10 depicts the DC voltages. Deviations in the DC voltages appear during the transient when using Q-LWAF, due to the auxiliary P control strategy used to estimate the WAF.

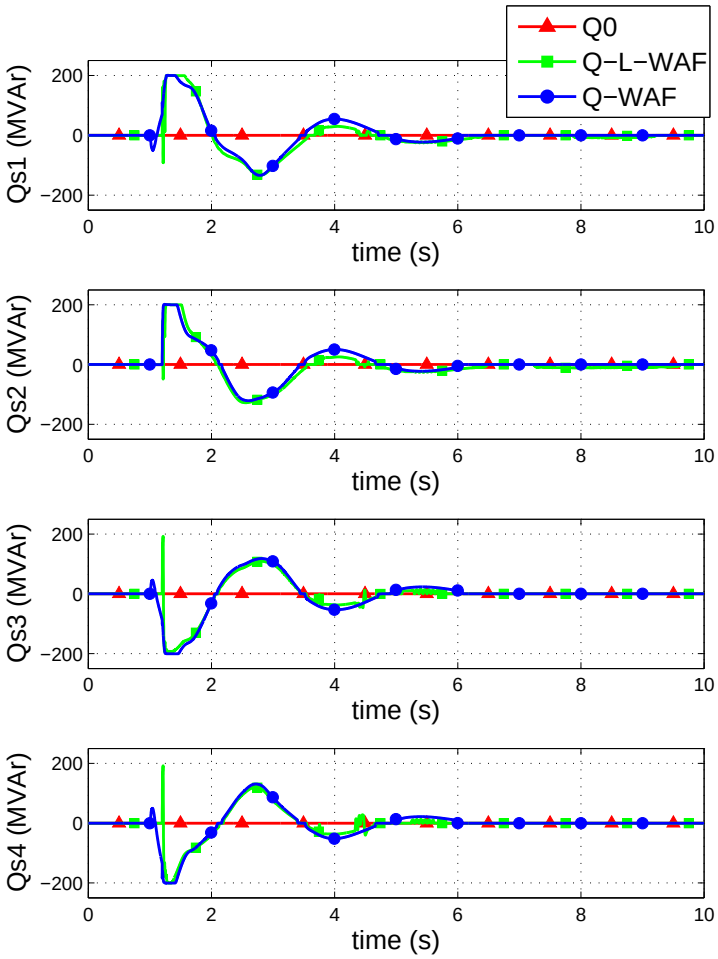

Fig. 7: Fault simulation. Reactive power injections ($Q_{s,i}$).

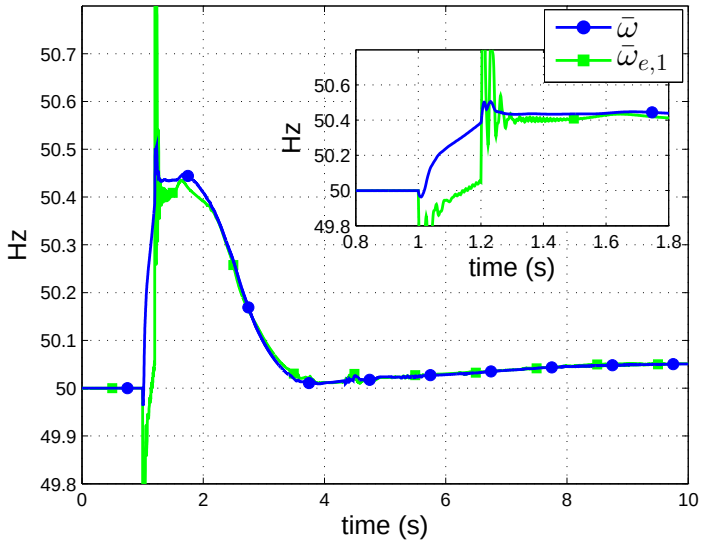

Fig. 8: Fault simulation. Q-LWAF: weighted-average frequency of the VSC-MTDC: true ($\bar{\omega}$) and estimated by VSC1 ($\bar{\omega}_{e,1}$).

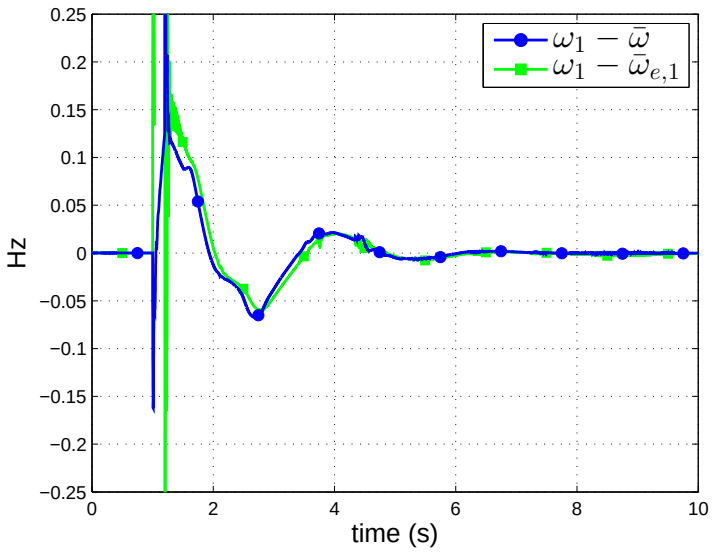

Fig. 9: Fault simulation. Q-LWAF: frequency deviation in VSC1 with respect to the true WAF ($\omega_1 - \bar{\omega}$) and with respect to the estimated WAF ($\omega_1 - \bar{\omega}_{e,1}$).

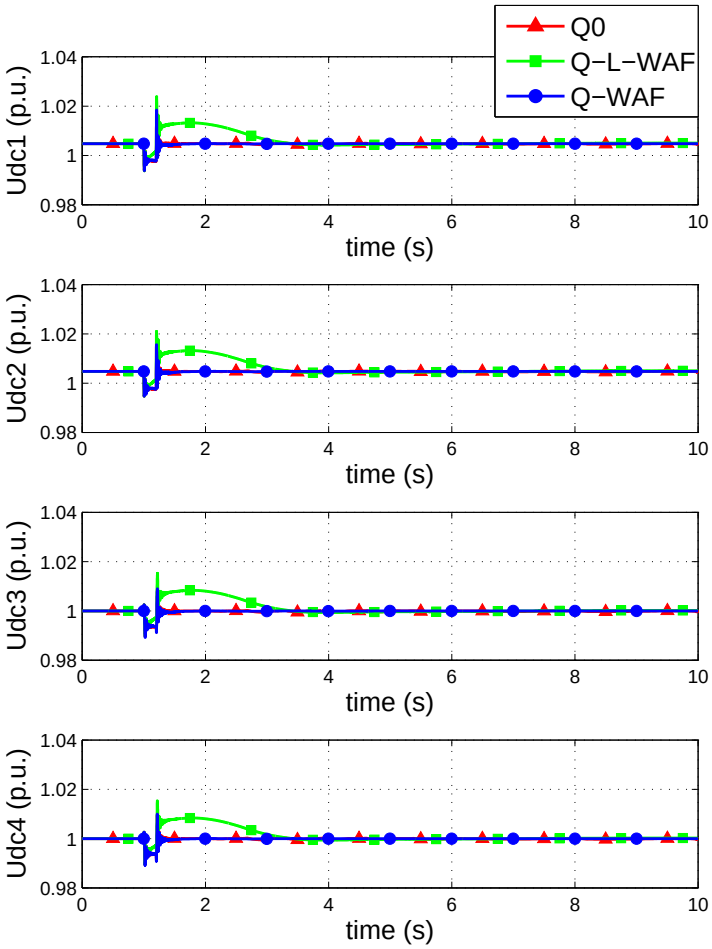

Fig. 10: Fault simulation. DC voltages ($u_{dc,i}$).

B. Detailed analysis of the local estimation of the weighted-average frequency

This subsection provides further details of the local estimation of the weighted-average frequency (WAF) by each VSC station in the proposed strategy Q-LWAF. All the results presented in Figs. 11-13 were obtained for the same fault as in the previous subsection and using local strategy Q-LWAF.

Firstly, frequency deviations at the converter stations with respect to the true WAF ($\omega_i - \bar{\omega}$) and with respect to the estimated WAF used in Q-LWAF ($\omega_i - \bar{\omega}_{e,i}$) are compared in Fig. 11. Results show that frequency deviations with respect to the true WAF and to the estimated WAF are very similar and follow the same pattern. This proves that local estimation of the WAF by each VSC station can be used for Q modulation (strategy Q-LWAF), as previously shown in Fig. 7.

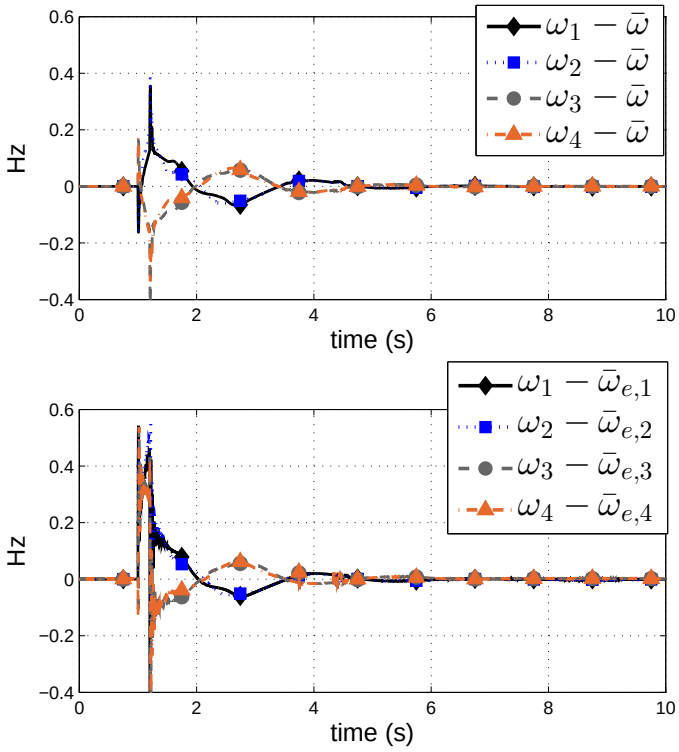

Fig. 11: Fault simulation. Q-LWAF. Frequency deviations with respect to the (upper plot) true and to the (lower plot) estimated weighted-average frequency.

Each converter is able to estimate the WAF using local measurements by means of auxiliary active-power control strategy P-LF (Fig. 4 with $\omega^* = 1$ p.u.). Supplementary P set points used by the VSCs are shown in Fig. 12. The mechanism for the local estimation of the WAF can be summarised as follows:

- Following the fault, frequency at each VSC station rises above the nominal frequency ($\omega_0 = 1$ p.u.). Therefore, according to Fig. 4, the AC-side P supplementary set point for each VSC ($\Delta p_{s,i}^{ref}$) decreases (see Fig. 12).
- The reduction of the AC-side P set point for each one of the VSC stations provokes the response of the DC-side control strategy in the opposite direction (the DC-voltage droop of Fig. 4), to maintain the DC-grid voltage. This means that all VSC stations increase their supplementary set point $\Delta p_{s,i}^{ref,DC}$ of Fig. 4, as shown in Fig. 12.
- As a result of the interaction of the AC- and DC-side P control strategies, each VSC has a total P set point $p_{s,i}^* = p_{s,i}^{ref} + p_{s,i}^{ref,DC}$, which is much smaller, in absolute value, than either $\Delta p_{s,i}^{ref}$ or $\Delta p_{s,i}^{ref,DC}$ (Fig. 12). The total supplementary P set point is shown in Fig. 13. The total P set point, $\Delta p_{s,i}^*$, increases in those VSC stations with frequency below the estimated weighted-average one and it decreases in those with frequency above.
- This mechanism allows each converter to estimate the WAF by using (9): only local measurements are required.

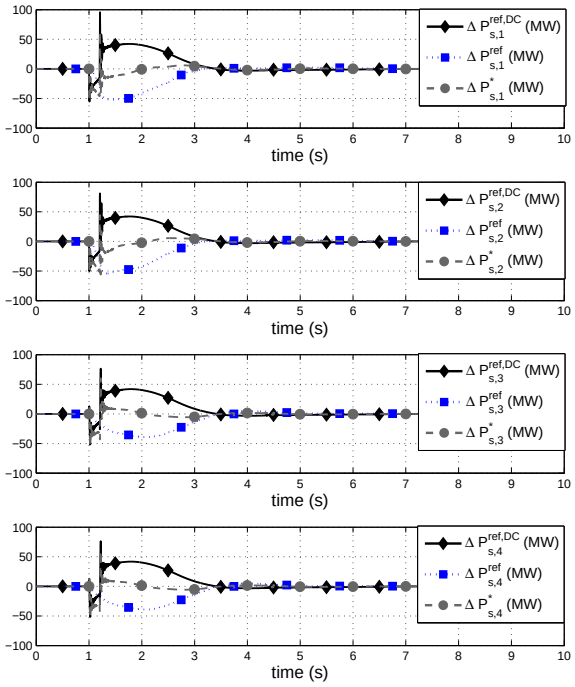

Fig. 12: Fault simulation. Q-LWAF. Supplementary P set points of the VSC stations.

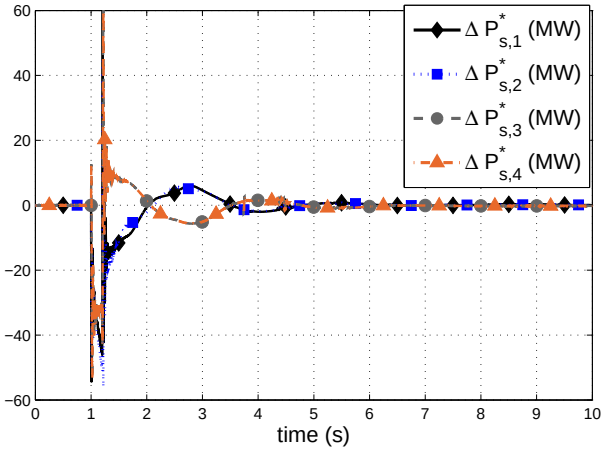

Fig. 13: Fault simulation. Q-LWAF. Total P supplementary set point of the VSC stations (detail).

C. Critical clearing times

Table II collects the critical clearing times (CCTs) of the faults described in Table I. Fault II has been selected in order to evaluate the performance of the proposed local strategy, Q-LWAF, under its most challenging conditions: Fault II is applied to bus 5, provoking that THE current limit of VSC1 is reached and the fault is very close to generator G1, which will accelerate very quickly. Since strategy Q-LWAF is only activated when ($u_{s,i} \geq V_{TH}$), i.e. after the fault clearing, its control actions will have less impact than strategy Q-WAF, which is considered the benchmark of achievable improvements. For comparison purposes, the impact of communication latency is also analysed for global strategy Q-WAF, which uses global measurements of the frequencies of the VSCs to calculate the weighted-average frequency in (2). In strategy Q-WAF, the frequency at terminal i measured by VSC j (ω_i^j)

will be delayed as:

$$\omega_i^j = \omega_i e^{-\tau_{ij} s},\ \tau_{ij} = \tau_{ij}^0 + \tau_{ij}^X = \tau_{ij}^0 \pm \Delta\tau, \tag{10}$$

where τ_{ij}^0 is a constant delay ($\tau_{ii}^0 = 0$ for $i = j$) and τ_{ij}^X is a stochastic random delay which follows a triangular distribution with upper/lower limits $\pm\Delta\tau$ and centred at zero. The delay was implemented in PSS/E by using a second-order Padé's approximation.

Both control strategies, global Q-WAF and local Q-LWAF, increase significantly the CCT of Fault I in comparison with the base case Q0. Strategies Q-WAF and Q-LWAF increase the CCT of Fault I from 103 ms to 356 ms and 240 ms, respectively (see Table II). The CCT obtained with strategy Q-WAF is greater than the one obtained with strategy Q-LWAF, since the latter acts after the fault clearing and converters reach their current limit during the fault. The performance of strategy Q-WAF deteriorates as the delay of communication latency increases. For communication delays of 50 ± 10ms and 100 ± 20ms, the CCT obtained with the proposed local strategy Q-LWAF is greater than the one obtained with global strategy Q-WAF.

Marginal improvents are obtained with the proposed local strategy Q-LWAF for Fault II (CCT is increased from 157 ms to 184 ms) and better results are obtained with global strategy Q-WAF, even with communication delays (Table II). This is due to the fact that strategy Q-LWAF works after the fault clearing, due to threshold V_{TH}. Nevertheless, the CCT is increased in comparison with the base case.

TABLE I: Fault description

	Short circuit at line $i-j$	close to bus	clearing
Fault I	7-8a	7	Disconnect 7-8a
Fault II	5-6	5	short circuit cleared (line not disconnected)

TABLE II: CCTs for simulated tests

CCT (ms)	Q0	global Q-WAF	with 50 ± 10ms	delay 100 ± 20ms	local Q-LWAF
Fault I	103	356	240	195	258
Fault II	157	335	269	230	184

D. Comparison with other control strategies

The proposed local control strategy Q-LWAF is now compared with different control strategies in VSC-MTDC systems for transient stability improvement proposed in previous work. The following cases are compared:

- Q0: Constant reactive-power injections.
- Q-WAF: Reactive-power injection based on the weighted-average frequency of the converter stations (global measurements) [14].
- Q-LWAF: Reactive-power injection based on the estimated weighted-average frequency of the converter stations using local measurements
- P-WAF: Active-power injection based on the weighted-average frequency of the converter stations (global measurements) [12].
- PQ-WAF: Strategies P-WAF and Q-WAF together (active- and reactive-power injections together) (global measurements) [14].
- TO-CLF: Time-optimal control Lyapunov's function, bang-bang control strategy for the active-power injections based on the speed deviations of the generators with respect to the speed of the COI (global measurements) [11].
- Q-FRT: Reactive-power support during faults (Fault Ride Through Capability, FRT) of type-4 generators required by Spanish Grid Code (local measurements) [18]. This strategy consists on a classical fast voltage support by means of increasing reactive current during the fault.

A brief description and data of the additional control strategies included in this analysis are provided in Section B of the Appendix, while further details are referred to the original references. In strategy TO-CLF, power control was

installed in VSC1, VSC2 and VSC3, while VSC4 controls the DC voltage (DC slack). This is a requirement of this control strategy. In all the other control strategies, VSC stations have the DC-voltage droop control implemented, as done in previous sections.

Table III shows the CCTs of the faults in Table II, obtained with the different control strategies. Significant improvements are obtained with global control strategies, either modulating P injections (P-WAF and TO-CLF), Q injections (Q-WAF) or both, P and Q injections (PQ-WAF). The best results are obtained with strategy PQ-WAF, since converters take advantage of modulating active- and reactive-power injections. Local strategy Q-FRT does not increase the CCTs. It is well known that FRT capability Q-FRT will help to improving transient stability of a nearby generator, since a VSC increases its reactive power injection during the fault, increasing therefore the electromagnetic torque seen by the generator. However, contrary to popular opinion, transient stability of a multi-machine system is a global problem and an effective control should increase the electromagnetic torque of those generators that have an excessively high speed during the transient (in order to slow them down),while decrasing the electromagnetic torque of the ones that havean excessively low speed during the transient (in order to accelerate them). As a results, generator are pulled together. This is, in fact, the philosophy behind global strategies (Q-WAF, P-WAF, PQ-WAF and TO-CLF) and local strategy Q-LWAF. Due to the estimation of the WAF, local strategy Q-LWAF also produce important improvements. As discussed in previous sections, the achievable improvement with Q-LWAF might be marginal for some type of faults very close to the AC terminal of a VSC (such as Fault II of Table I).

TABLE III: CCTs for simulated tests

CCT (ms)	Q0	global Q-WAF	local Q-LWAF	global P-WAF	global PQ-WAF	global TO-CLF	local Q-FRT
Fault I	103	356	258	441	507	313	98
Fault II	157	335	184	229	323	242	160

In comparison with the control approaches proposed previously, the local control strategy proposed in this work, Q-LWAF, has the following advantages:

- It is communication free. Therefore, it does not present potential problems associated to communication latency and no additional investment in a fast communication system is required.
- Due to the local estimation of the WAF by each converter, the strategy produces significant improvements, similar to the ones obtained with global measurements.
- Each VSC station modulates its Q injection. Although results show that significant improvements can also be achieved by modulating P injections, Q-based control strategies in VSC-MTDC systems may be easier to implement, in practice, due to the following reasons:
  - Q-based control strategies are simpler than P-based control strategies, since the former do not affect either the power balance and or the DC voltages in the VSC-MTDC system.
  - TSOs might prefer Q-based rather than P-based strategies, since, in the former, P injections of the VSC stations will be kept constant and equal to their programmed set points (only Q injections are modulated to improve transient stability). Although in the proposed approach, P injections are modulated for estimation purposes, this P modulation is of a small amplitude.

V. Case study

Various Q-control strategies have been tested and compared by simulation using PSS/E and the Nordic32A grid modified with a VSC-HVDC 3-terminal system, as shown in Fig. 14. System data can be found in [42]. The load in the central area has been increased in order to consider a heavily loaded scenario, as detailed in Section A-2 of the Appendix. Parameters of VSC stations and DC grid are provided in Table VI.

The initial operating point of the MTDC system was set as:

- VSC1: $P^0_{s,1} = -350$ MW and $Q^0_{s,1} = 0$ MVAr.
- VSC2: $P^0_{s,2} = 500$ MW and $Q^0_{s,2} = 150$ MVAr.
- VSC3: $u^0_{dc,3} = 1$ p.u and $Q^0_{s,3} = 100$ MVAr (VSC3 is used as the DC-slack converter for power-flow calculation of the initial operating point).

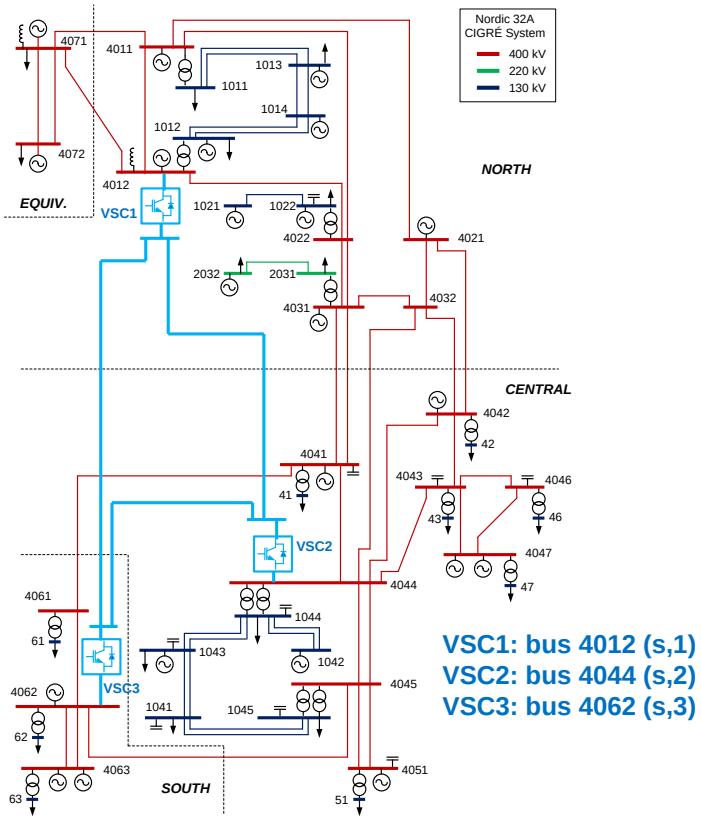

Fig. 14: Nordic 32A system + a VSC-MTDC system.

The following strategies will be compared under severe three-phase short circuits:

- Q0: Constant reactive-power injections.
- Q-WAF: Reactive-power injection based on the weighted-average frequency of the converter stations (global measurement) (Fig. 3), with parameters: $k_{Q,i} = 200$ p.u, $T_{f,i} = 0.1$ s, $T_{W,i} = 15$ s, $\Delta q_{max,i} = 1$ p.u and $\alpha_k = 1/3$. The gains are in nominal p.u. The frequency set point is computed as (2).
- Q-LWAF: Reactive-power injection based on the estimated weighted-average frequency of the converter stations using local measurements, with parameters:
  - Q modulation (Fig. 3): $k_{Q,i} = 200$ p.u, $T_{f,i} = 0.01$ s, $T_{W,i} = 15$ s, $\Delta q_{max,i} = 1$ p.u, $V_{TH,i} = 0.60$ p.u and $\alpha_k = 1/3$. The frequency set point is computed as in (9).
  - P modulation, for estimation purposes (Fig. 4 with $\omega^* = 1$ p.u.): $k_{P,i} = 10$ p.u, $T_{f,i} = 0.1$ s, $T_{W,i} = 15$ s, $\Delta p_{max,i} = 1$ p.u and $k_{dc,i} = 0.1$ p.u. The frequency set point is $\omega_i^* = 1$ p.u (P-LF).

A. Fault simulation

A three-phase-to-ground short circuit has been applied to line 4031-4041a (close to bus 4041) at $t = 1$s and the fault was cleared after 300 ms disconnecting both circuits of the corridor 4031-4041 a & b. The difference between the rotor angles of generators G4012 (North) and G4062 (South) is shown in Fig. 15. Synchronism is lost for constant Q control (Q0), whilst synchronism is maintained with global control strategy Q-WAF and with the local control strategy proposed in this work Q-LWAF, producing, both, a very similar response.

The reactive-power injections of the converters are shown in Fig 16. Using strategies Q-WAF and Q-LWAF, the reactive-power injection of each converter is modulated, stabilising the system. In both cases, during the transient, the reactive-power injection is increased (reduced) in those terminals with frequency above (below) the weighted-average frequency of the MTDC system. This slows down (accelerates) nearby generators, helping to maintain the synchronism of the system. Fig. 16 shows that the Q modulation in strategy Q-LWAF is very similar to the one produced by strategy Q-WAF. The latter uses as frequency set point the weighted-average frequency and the

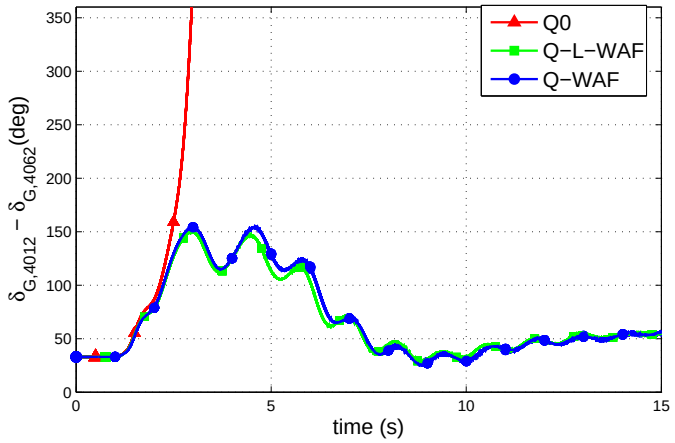

Fig. 15: Fault simulation. Generator angles.

former estimates that signal using local measurements at each converter station thanks to the (small) active-power modulation produced by strategy P-LF. The weighted-average frequency estimated by VSC1 ($\bar{\omega}_{e,1}$), using (9), is compared with the true value ($\bar{\omega}$) in Fig 17, showing good agreement. Fig. 18 compares the frequency deviation in VSC1, with respect to the true WAF ($\omega_1 - \bar{\omega}$) and with respect to the estimated WAF ($\omega_1 - \bar{\omega}_{e,1}$, in Q-LWAF). Since both signals are very similar, Q modulation in strategies Q-WAF and Q-LWAF will also present as similar behaviour.

Finally, the DC-voltages of the DC grid are shown in Fig 19. They remain almost constant with strategies Q0 and Q-WAF, while strategy Q-LWAF produces DC-voltage deviations during the transient. Gains $k_{P,i}$ of strategy P-LF (in Q-LWAF) should be small enough to ensure admissible DC-voltage fluctuations during transients. Naturally, droop constants ($k_{dc,i}$) also could be modified to reduce DC-voltage deviations.

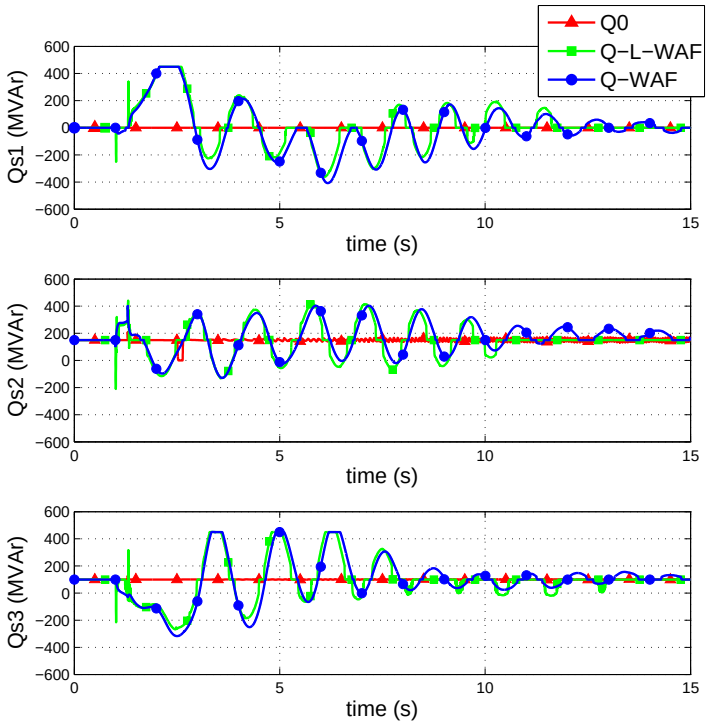

Fig. 16: Fault simulation. Reactive power injections ($Q_{s,i}$).

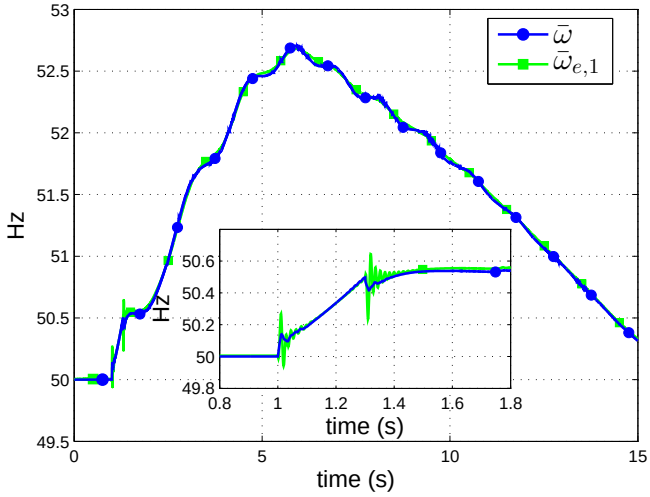

Fig. 17: Fault simulation. Q-LWAF: weighted-average frequency of the VSC-MTDC: true ($\bar{\omega}$) and estimated by VSC1 ($\bar{\omega}_{e,1}$).

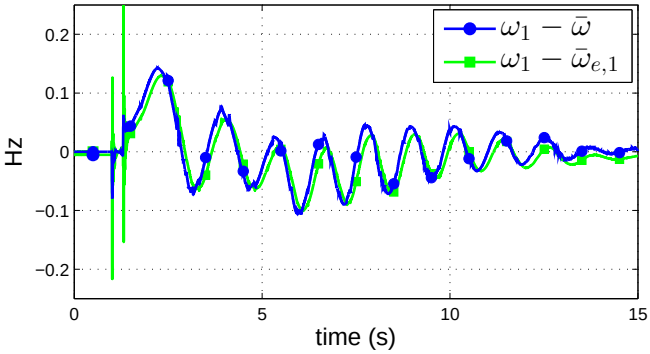

Fig. 18: Fault simulation. Q-LWAF: frequency deviation in VSC1 with respect to the true WAF ($\omega_1 - \bar{\omega}$) and with respect to the estimated WAF ($\omega_1 - \bar{\omega}_{e,1}$).

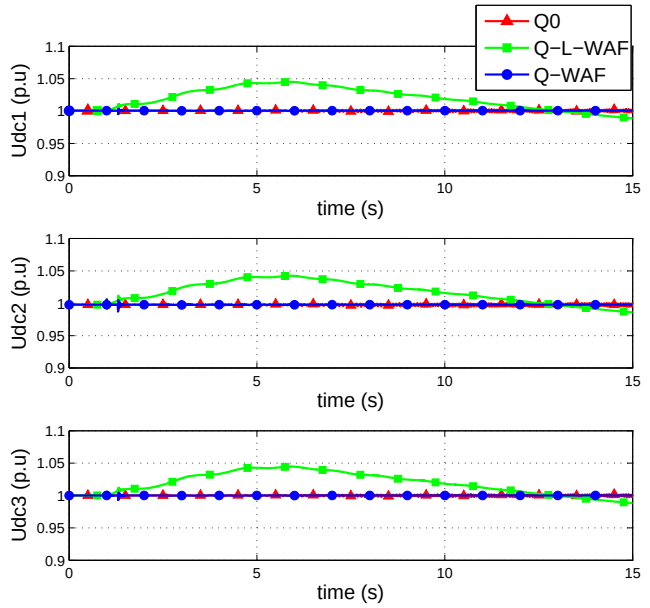

Fig. 19: Fault simulation. DC voltages ($u_{dc,i}$).

B. Critical clearing times

Several faults (described in Table IV) have been simulated and their CCTs have been evaluated and collected in Table V. Both strategies, global Q-WAF and local Q-LWAF, increase the CCTs in comparison with the base case Q0. For some faults, the CCT is increased significantly. For example, the CCT of Fault I is increased from 105 ms to 370 ms with Q-WAF and to 379 ms with Q-LWAF (very similar figures are obtained with both strategies). The slightly longer CCT obtained with the latter is probably due to the (small) help of the P-LF modulation when estimating $\bar{\omega}$.

The CCTs with Faults II and IV are also increased with strategies Q-WAF and Q-LWAF, but the best results are now obtained with the former. These scenarios have in common that faults are very close to the converters and the current limit of some converters are reached during the short circuit. When limits are reached, the converters do not estimate the weighted-average frequency properly with strategy Q-LWAF and better results are obtained using global measurements (Q-WAF). Nevertheless, local Q-LWAF proves to be robust.

The performance of global strategy Q-WAF deteriorates with communication latency and longer CCTs are obtained with proposed local strategy Q-LWAF, in almost all cases (see Table V). Noticeably, the CCT of Fault IV presents a different pattern in the presence of communication latencies (in Q-WAF). This particular behaviour in Fault IV was already observed in [14].

TABLE IV: Fault description

	Short circuit at line $i-j$	close to bus	clearing
Fault I	4031-4041a	4041	Disconnect 4031-4041a&b
Fault II	4012-4022	4012	Line disconnected
Fault III	4012-4022	4022	Line disconnected
Fault IV	4032-4044	4044	Line disconnected
Fault V	4011-4022	4011	Line disconnected

TABLE V: CCTs for simulated tests

CCT (ms)	Q0 Q0	global Q-WAF	with 50 ± 10ms	delay 100 ± 20ms	local Q-LWAF
Fault I	105	370	320	171	379
Fault II	188	247	235	225	214
Fault III	237	253	248	243	251
Fault IV	390	564	581	603	519
Fault V	205	250	240	231	224

VI. Conclusions

This paper proposes and analyses a communication-free reactive-power control strategy (Q-LWAF) of a VSC-HVDC multi-terminal system for transient stability improvement in hybrid AC-DC transmission systems. The proposed control strategy was inspired by one using the weighted-average frequency of the VSC-MTDC's converter stations as frequency set point (communications are required) of a supplementary reactive-power controller for each converter station (Q-WAF). In the reactive-power control law derived in this work, an active-power control strategy using local measurements of the frequency at each converter station is also implemented (using small gains), in addition to the DC-voltage droop control. The small (local) active-power modulation is then used to estimate the weighted-average frequency of the VSC-MTDC system and this signal is used as the frequency set point of a reactive-power control strategy.

Results showed that the proposed reactive-power control strategy improves transient stability, significantly, and increases the Critical Clearing Times (CCTs) of a set of faults. It behaves similarly to strategy Q-WAF but only local measurements at the converter stations are required.

REFERENCES

[1] E. Bompard, G. Fulli, M. Ardelean, and M. Masera, "It's a Bird, It's a Plane, It's a... Supergrid," *IEEE power & energy magazine*, vol. 12, no. 2, pp. 41–50, 2014.

[2] N. Flourentzou, V. G. Agelidis, and G. D. Demetriades, "VSC-Based HVDC Power Transmission Systems: An Overview," *IEEE Transactions on Power Electronics*, vol. 24, no. 3, pp. 592–602, 2009.

[3] P. Kundur, J. Paserba, V. Ajjarapu, G. Andersson, A. Bose, C. Canizares, N. Hatziargyriou, D. Hill, A. Stankovic, C. Taylor, T. Van Cutsem, and V. Vittal, "Definition and classification of power system stability IEEE/CIGRE joint task force on stability terms and definitions," *IEEE Transactions on Power Systems*, vol. 19, no. 3, pp. 1387–1401, 2004.

[4] M. Pertl, T. Weckesser, M. Rezkalla, and M. Marinelli, "Transient stability improvement: a review and comparison of conventional and renewable-based techniques for preventive and emergency control," *Electrical Engineering*, vol. 100, no. 3, pp. 1701–1718, 2018.

[5] R. Shah, J. Sánchez, R. Preece, and M. Barnes, "Stability and control of mixed AC-DC systems with VSC-HVDC: a review," *IET Generation Transmission and Distribution*, vol. 12, no. 10, pp. 2207–2219, 2017.

[6] H. Latorre, M. Ghandhari, and L. Söder, "Active and reactive power control of a VSC-HVdc," *Electric Power Systems Research*, vol. 78, no. 10, pp. 1756–1763, 2008.

[7] A. Fuchs, M. Imhof, T. Demiray, and M. Morari, "Stabilization of Large Power Systems Using VSC - HVDC and Model Predictive Control," *IEEE Transactions on Power Delivery*, vol. 29, no. 1, pp. 480–488, 2014.

[8] L. Sigrist, F. Echavarren, L. Rouco, and P. Panciatici, "A fundamental study on the impact of HVDC lines on transient stability of power systems," in *Proc. IEEE/PES PowerTech Conference, Eindhoven, Netherlands*, 2015, pp. 1–6.

[9] I. Martínez Sanz, B. Chaudhuri, and G. Strbac, "Coordinated Corrective Control for Transient Stability Enhancement in Future Great Britain Transmission System," in *Proc. 19th Power Systems Computation Conference (PSCC), Genoa, Italy*, 2016, pp. 1–7.

[10] J. Machowski, P. Kacejko, L. Nogal, and M. Wancerz, "Power system stability enhancement by WAMS-based supplementary control of multi-terminal HVDC networks," *Control Engineering Practice*, vol. 21, no. 5, pp. 583–592, May 2013.

[11] R. Eriksson, "Coordinated Control of Multiterminal DC Grid Power Injections for Improved Rotor-Angle Stability Based on Lyapunov Theory," *IEEE Transactions on Power Delivery*, vol. 29, no. 4, pp. 1789–1797, 2014.

[12] J. Renedo, A. García-Cerrada, and L. Rouco, "Active Power Control Strategies for Transient Stability Enhancement of AC/DC Grids With VSC-HVDC Multi-Terminal Systems," *IEEE Transactions on Power Systems*, vol. 31, no. 6, pp. 4595–4604, 2016.

[13] G. Tang, Z. Xu, H. Dong, and Q. Xu, "Sliding Mode Robust Control Based Active-Power Modulation of Multi-Terminal HVDC Transmissions," *IEEE Transactions on Power Systems*, vol. 31, no. 2, pp. 1614–1623, 2016.

[14] J. Renedo, A. García-Cerrada, and L. Rouco, "Reactive-Power Coordination in VSC-HVDC Multi-Terminal Systems for Transient Stability Improvement," *IEEE Transactions on Power Systems*, vol. 32, no. 5, pp. 3758–3767, 2017.

[15] O. Kotb, M. Ghandhari, R. Eriksson, R. Leelarujic, and V. K. Sood, "Stability enhancement of an interconnected AC/DC power system through VSC-MTDC operating point adjustement," *Electric Power Systems Research*, vol. 151, pp. 308–318, 2017.

[16] European Comission , *Comission Regulation (EU) 2016/631 of 14 April 2016. Establishing a network code on requirements for grid connection of generators*. Official Journal of the European Union, 2016.

[17] European Comission, *Comission Regulation (EU) 2016/1447 of 26 August 2016. Establishing a network code on requirements for grid connection of high voltage direct current systems and direct current-connected power park modules*. Official Journal of the European Union, 2016.

[18] Ministerio de Industria, Turismo y Comercio, Gobierno de España, *P. O. 12.3. Requisitos de respuesta frente a huecos de tensión de las instalaciones eólicas*. BOE no. 254, Spain, Online: www.boe.es/boe/dias/2006/10/24/pdfs/A37017-37019.pdf (accessed: 10-02-2019), pp. 37017–37019, 2006.

[19] N. R. Trinh, I. Erlich, M. Zeller, and K. Wuerflinger, "Enhancement of grid transient stability using MMC-VSCH-VDC control," in *Proc. 11th IET Conference on AC and DC Power Transmission, Birmingham, UK*, 2015, pp. 1–6.

[20] X. Fan, J. Shu, and B. Zhang, "Coordinated Control of DC Grid and Offshore Wind Farms to Improve Rotor-Angle Stability," *IEEE Transactions on Power Systems*, vol. 33, no. 4, pp. 4625–4623, 2018.

[21] K. Sun, Y. Xing, and J. M. Guerrero, "A Distributed Control Strategy Based on DC Bus Signaling for Modular Photovoltaic Generation Systems With Battery Energy Storage," *IEEE Transactions on Power Electronics*, vol. 26, no. 10, pp. 3032–3045, 2011.

[22] C. N. Papadimitriou, V. A. Kleftakis, A. Rigas, and N. D. Hatziargyriou, "A DC-microgrid control strategy using DC- bus signaling," in *Proc. MedPower, Athens, Greece*, 2014, pp. 1–8.

[23] T. Haileselassie, K. Uhlen, and T. Undeland, "Control of Multiterminal HVDC Transmission for Offshore Wind Energy," in *Proc. Nordic Wind Power Conference, Ronne, Denmark*, 2009, pp. 1–7.

[24] E. Prieto-Araujo, F. D. Bianchi, A. Junyent-Ferré, and O. Gomis-Bellmunt, "Methodology for Droop Control Dynamic Analysis of Multiterminal VSC-HVDC Grids for Offshore Wind Farms," *IEEE Transactions on Power Delivery*, vol. 26, no. 4, pp. 2476–2485, 2011.

[25] A. Egea-Alvarez, F. Bianchi, A. Junyent-Ferré, G. Gross, and O. Gomis-Bellmunt, "Voltage Control of Multiterminal VSC-HVDC Transmission Systems for Offshore Wind Power Plants : Design and Implementation in a Scaled Platform," *IEEE Transactions on Industrial Electronics*, vol. 60, no. 6, pp. 2381–2391, 2013.

[26] T. K. Vrana, J. Beerten, R. Belmans, and O. B. Fosso, "A classification of DC node voltage control methods for HVDC grids," *Electric Power Systems Research*, vol. 103, pp. 137–144, Oct. 2013.

[27] T. M. Haileselassie and K. Uhlen, "Primary frequency control of remote grids connected by multi-terminal HVDC," in *Proc. IEEE/PES General Meeting, Providence, RI, USA*, 2010, pp. 1–6.

[28] B. Silva, C. L. Moreira, L. Seca, Y. Phulpin, and J. A. Peças Lopes, "Provision of Inertial and Primary Frequency Control Services Using Offshore Multiterminal HVDC Networks," *IEEE Transactions on Sustainable Energy*, vol. 3, no. 4, pp. 800–808, 2012.

[29] N. R. Chaudhuri, R. Majumder, and B. Chaudhuri, "System Frequency Support Through Multi-Terminal DC (MTDC) Grids," *IEEE Transactions on Power Systems*, vol. 28, no. 1, pp. 347–356, 2013.

[30] S. Akkari, J. Dai, M. Petit, and X. Guillaud, " Interaction between the voltage-droop and the frequency-droop control for multi-terminal HVDC systems," *IET Generation, Transmission & Distribution*, vol. 10, no. 6, pp. 1345–1352, 2016.
[31] R. Eriksson, "A New Control Structure for Multi-Terminal dc Grids to Damp Inter-Area Oscillations," *IEEE Transactions on Power Delivery*, vol. 31, no. 3, pp. 990–998, 2016.
[32] S. Cole, J. Beerten, and R. Belmans, "Generalized Dynamic VSC MTDC Model for Power System Stability Studies," *IEEE Transactions on Power Systems*, vol. 25, no. 3, pp. 1655–1662, 2010.
[33] J. Beerten, S. Cole, and R. Belmans, "Modeling of Multi-Terminal VSC HVDC Systems With Distributed DC Voltage Control," *IEEE Transactions on Power Systems*, vol. 29, no. 1, pp. 34–42, 2014.
[34] S. Liu, Z. Xu, W. Hua, G. Tang, and Y. Xue, "Electromechanical Transient Modeling of Modular Multilevel Converter Based Multi-Terminal HVDC Systems," *IEEE Transactions on Power Systems*, vol. 29, no. 1, pp. 72–83, 2014.
[35] G. Daelemans, K. Srivastava, M. Reza, S. Cole, and R. Belmans, " Minimization of steady-state losses in meshed networks using VSC HVDC," in *Proc. IEEE/PES General Meeting, Calgary, AB, Canada*, 2009, pp. 1–5.
[36] Y. Zhou, H. Huang, Z. Xu, W. Hua, F. Yang, and S. Liu, "Wide-area measurement system-based transient excitation boosting control to improve power system transient stability," *IET Generation, Transmission & Distribution*, vol. 9, no. 9, pp. 845–854, 2015.
[37] L. Díez-Maroto, L. Vanfretti, M. S. Almas, G. M. Jónsdóttir, and L. Rouco, "A WACS exploiting generator Excitation Boosters for power system transient stability enhancement," *Electric Power Systems Research*, vol. 148, pp. 245–253, 2017.
[38] L. Díez-Maroto, J. Renedo, L. Rouco, and F. Fernández-Bernal, "Lyapunov Stability Based Wide Area Control Systems for Excitation Boosters in Synchronous Generators," *IEEE Transactions on Power Systems*, vol. 34, no. 1, pp. 194–204, 2019.
[39] R. Eriksson, J. Beerten, and M. Ghandhari, "Optimizing DC Voltage Droop Settings for AC/DC System Interactions," *IEEE Transactions on Power Delivery*, vol. 29, no. 1, pp. 362–369, 2014.
[40] P. Kundur, *Power System Stability and Control*. McGraw Hill Education, 1993.
[41] J. Renedo, A. García-Cerrada, L. Rouco, L. Sigrist, I. Egido, and S. Sanz Verdugo, "Development of a PSS/E tool for power-flow calculation and dynamic simulation of VSC-HVDC multi-terminal systems," in *Proc. 13th IET International Conference on AC and DC Power Transmission, Manchester, UK*, 2017, pp. 1–6.
[42] M. Stubbe (Convener), "Long Term Dynamics Phase II," Cigré Task Force 38.02.08 - TB 102, Tech. Rep., 1995.
[43] Siemens-PTI, *PSS/E 33.5 Model Library*, 2013.
[44] T. Van Cutsem and L. Papangelis, "Description, Modeling and Simulation Results of a Test System for Voltage Stability Analysis," Université de Liège, Belgium, Tech. Rep., 2014.
[45] B. Karlsson, "Comparison of PSSE & PowerFactory," Degree Project, Uppsala Universitet, Uppsala, Sweden, 2013.

APPENDIX

A. Details of the case studies

1) Kundur's two-area test system: Data of the HVAC system can be found in [40], with the only difference that, here, the nominal voltage of the transmission system and the nominal frequency have been changed to 220 kV and 50 Hz, respectively. Synchronous machines are represented by a 6th-order dynamic model. All parameters read:

$$\begin{aligned}
&S_N = 900 \text{ MVA},\ H = 4.5 \text{ s (G1, G2)},\ H = 6.175 \text{ s (G3, G4)},\ ,\ D = 0,\ T'_{d0} = 8 \text{ s},\ T''_{d0} = 0.03 \text{ s},\\
&T'_{q0} = 0.4 \text{ s},\ T''_{q0} = 0.05 \text{ s},\ X_d = 1.8 \text{ p.u},\ X_q = 1.7 \text{ p.u},\ X'_d = 0.3 \text{ p.u},\ X'_q = 0.55 \text{ p.u},\\
&X''_d = X''_q = 0.25 \text{ p.u},\ \ X_l = 0.2 \text{ p.u},\ \ S(1.0) = 0.0435 \text{ p.u},\ \ S(1.2) = 0.2963 \text{ p.u}.
\end{aligned} \tag{11}$$

Generators have a bus-fed static excitation system (Fig. 20), with parameters: $T_R = 0.01$ s, $K_A = 200$ p.u, $K_C = 0$ p.u, $E_{EMAX} = 6.4$ p.u, $E_{EMIN} = -6.4$ p.u, $E_{FDmax} = 6.4$ p.u, $E_{FDmin} = -6.4$ p.u. The generators are also equipped with a power system stabiliser (PSS) (Fig. 21), with parameters: $K/T = 20$ s^{-1}, $T = 10$ s, $T_1/T_3 = 2.5$, $T_3 = 0.02$ s $T_2/T_4 = 0.5555$, $T_4 = 5.4$ s and $H_{LIM} = 0.05$ p.u. The governor system is shown in Fig. 22 and the parameters used read:

$$\begin{aligned}
&K = 20 \text{ p.u},\ T_1 = T_2 = 0 \text{ s},\ \ T_3 = 0.3 \text{ s},\ \ U_o = 1 \text{ p.u./s},\ \ ,U_c = -1 \text{ p.u./s},\ \ P_{MAX} = 1 \text{ p.u},\ P_{MIN} = 0\text{p.u},\\
&T_4 = 0.3 \text{ s},\ K_1 = 0.3 \text{ p.u},\ K_2 = 0 \text{ p.u},\ T_5 = 7 \text{ s},\ K_3 = 0.3 \text{ p.u},\ K_4 = 0 \text{ p.u},\ T_6 = 0.6 \text{ s},\\
&K_5 = K_6 = K_7 = K_8 = 0 \text{ p.u},\ T_7 = 0 \text{ s}.
\end{aligned} \tag{12}$$

For dynamic simulation, loads are modelled as constant active current and constant impedance for the reactive-power part. The inertia of machines G1 and G2 has been reduced from 6.5 s to 4.5 s, in order to consider a more critical case for transient stability. In addition, load of bus 7 was transferred to bus 9, in order to consider a more critical case. Loads used are 467 MW and 100 MVAr at bus 7; and 2267 MW and 0 MVAr at bus 9. Data of the VSC-MTDC system are provided in Table VII. VSC stations operate with DC-voltage droop control and reactive-power control.

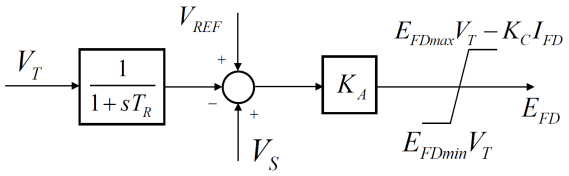

Fig. 20: Excitation system.

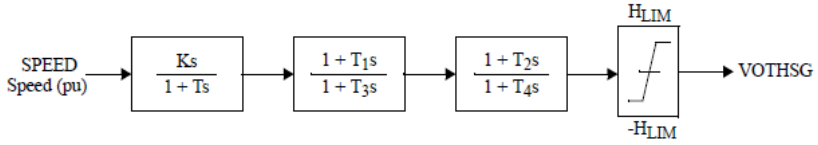

Fig. 21: Power System Stabiliser (STAB1). Figure from [43].

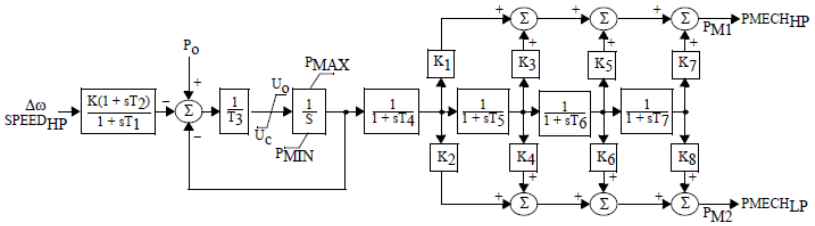

Fig. 22: Governor system (IEEEG1). Figure from [43].

TABLE VI: Converter and DC grid parameters

Parameters Converter rating are base values for p.u.	Two-area system (Section IV)	Nordic32A (Section V)
Rating VSC, DC voltage	500 MVA, ±320 kV	1000 MVA, ±320 kV
Max. active (reactive) power	±500 MW (±200 MVAr)	±1 GW (±450 MVAr)
Max. current	1 p.u (d-priority)	1 p.u (d-priority)
Max. DC voltage	±10 %	±10 %
Max. modulation index	1.19 p.u	1.19 p.u
Current-controller time constant (τ)	5 ms	5 ms
Connection resistance (r_s)/reactance (x_s)	0.002 p.u / 0.20 p.u	0.002 p.u / 0.17 p.u
P prop./int. control: ($K_{d,p1}/K_{d,i1}$)	0/0	0/0
Vdc prop./int. control ($K_{d,p2}/K_{d,i2}$)	2 p.u/0.12 p.u/s	2 p.u/0.12 p.u/s
Q-control prop./int. control: ($K_{q,p1}/K_{q,i1}$)	0/0	0/0
DC-voltage droop constant ($k_{dc,i}$)	0.1 p.u	0.1 p.u.
VSCs' loss coefficients (a/b) in p.u.	5.25/1.65 $\times 10^{-3}$ p.u.	11.03/3.464 $\times 10^{-3}$
VSCs' loss coefficients (c_{rec}/c_{inv}) in p.u.	2.10/3.14 $\times 10^{-3}$ p.u.	4.4/6.6 $\times 10^{-3}$
DC-bus capacitance ($C_{dc,i}$)	195 μF	195 μF
DC-line series parameters ($R_{dc,ij}/L_{dc,ij}$)	0.51 Ω/35.03 mH (lines 1-2 & 3-4) 5.23 Ω/357.26 mH (line 1-3) 4.92 Ω/336.24 mH (line 2-4)	2.05 Ω/140.1 mH

2) Cigré Nordic32A test system: Data of Cigré Noridc32A test system can be found in [42]. A comprehensive description of this test system can be found in [44] and [45]. Generators are represented with 6th-order models and their excitation system, PSS and governor (according to [42]). Dynamic simulations are carried out with constant impedance characteristic of loads. Modifications done in order to consider a more critical case are provided in Table VII. Data of the VSC-MTDC system are given in Table VI.

TABLE VII: Modifications of NORDIC32A case

		Original value	New value
Loads	bus 1044	800 MW	1300 MW
	bus 41	540 MW	620 MW
	bus 4071 (equiv.)	300 MW	0 MW
	bus 4072 (equiv.)	2000 MW	1840 MW
	bus 62	300 MW	200 MW
Shunts	buses 1044 and 4041	200 MVAr	300 MVAr

B. Additional control strategies used for further comparison

1) P-WAF [12]: In strategy P-WAF, each VSC station of the MTDC modulates its P injection according to Fig. 4, where the frequency set point is calculated as the weighted-average of the frequencies measured at the AC connection point of the VSC stations of the MTDC system (2). Parameters are set to $k_{P,i} = 200$ p.u, $T_{f,i} = 0.1$ s, $T_{W,i} = 15$ s, $\Delta p_{max,i} = 1$ p.u and $k_{dc,i} = 0.1$ p.u. The frequency set point is $\omega_i^* = \bar{\omega}_i$ p.u.

2) PQ-WAF [14]: Strategy PQ-WAF modulates P and Q injections of the VSC stations of the MTDC system, simultaneously, according to strategies P-WAF and Q-WAF, respectively. The same parameters used for strategies P-WAF and Q-WAF are used for this control strategy.

3) TO-CLF [11]: Time-optimal control Lyapunov's function (TO-CLF) strategy uses a so-called bang-bang controller for P injections of the VSC stations of the MTDC system. Each VSC j calculates the following value:

$$\phi(j) = -\sum_{\forall i} b_{P,ji} \left(\omega_{G,i} - \omega_{COI}\right) \tag{13}$$

where $b_{P,ji}$ quantifies the effect of a power injection using VSC j on the speed of the generator i ($\omega_{G,i}$) and ω_{COI} is the speed of the COI (see [11] for details). VSC j injects a fixed supplementary amount of active power $\Delta p_{s,j}^{ref}$ into the HVAC system according to:

$$\Delta p_{s,j}^{ref} = \begin{cases} +\Delta p_{max,j} & \text{if } \phi(j) > +\epsilon \\ -\Delta p_{max,j} & \text{if } \phi(j) < -\epsilon \\ 0 & \text{otherwise} \end{cases} \tag{14}$$

Parameters are set to $\epsilon = 0.001$ p.u. and $\Delta p_{max,j} = 100$ MW (this value of $\Delta p_{max,j}$ was used in [11]).

4) Q-FRT [18]: Strategy Q-FRTprovides the reactive-power support during faults (Fault Ride Through Capability, FRT) of type-4 generators required by Spanish Grid Code [18], and it has beens implemented in all the VSC stations of the MTDC in this work, when required. The strategy provides fast voltage support by means of increasing reactive current during the fault. Fig. 23 shows the required FRT curve. Reactive current must be above the curve during faults.

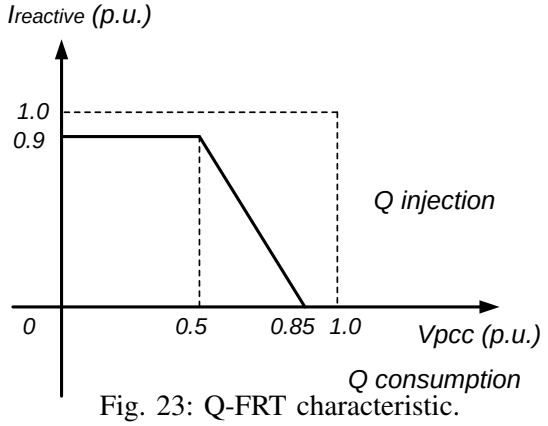

Fig. 23: Q-FRT characteristic.

AKNOWLEDGEMENTS

Work initially supported by the Spanish Government under Project ENE2014-57760-C2-1R of the Spanish RETOS programme and by Madrid Regional Government. under PRICAM-CM Project, Ref. S2013/ICE-2933. Work continues supported by PROMINT-CM Ref. S2018/EMT-4366, funded by Madrid Regional Government. Internal ref. of this article: IIT-17-005A.